

On the relation of the COVID-19 reproduction number to the explosive timescales: the case of Italy

Dimitris G. Patsatzis*

School of Chemical Engineering, National Technical University of Athens, 15780 Athens, Greece

Abstract

A great issue of discussion of an infectious disease is its basic reproduction number R_0 , which provides an estimation of the contagiousness of the disease. When $R_0 > 1$, the disease spread will potentially lead to an outbreak, such that of the ongoing COVID-19 pandemics. During the evolution of an outbreak, various non-pharmaceutical interventions are employed, the impact of which is frequently assessed by the reduction that they introduce to the effective reproduction number R_t ; reduction below 1 is an indication of eventual dying out of the disease spread. Motivated by the fact that R_0 essentially expresses the stability of the disease-free equilibrium, in this work, R_t was examined in the view of timescale analysis. It was shown that during the evolution of the COVID-19 outbreak in Italy, when various interventions were in place, R_t had a clear relation with the explosive timescale characterizing the dynamics of the outbreak. In particular, it is shown that the existence of an explosive timescale during the progression of the epidemics implies $R_t > 1$, while its absence implies $R_t < 1$. In addition, as this timescale converges/diverges with the immediately slowest one, R_t approaches to/withdraws from its threshold value 1. These results suggest that timescale analysis can be utilized for the assessment of the impact of various interventions, since it reflects the insight provided by the effective reproduction number, without being hindered by the selection of the population model, nor the parameter estimation process followed for model calibration.

Keywords: COVID-19, reproduction number, timescale analysis, population dynamics

1. Introduction

As of March 11, 2020, the novel coronavirus disease (COVID-19) was declared a pandemic by World Health Organization (WHO) [1]. By January 15, 2021, the COVID-19 pandemics has been spread to more than 219 countries and territories, reporting more than 93 million infected cases and 2 million deaths [2].

A great issue of discussion of the COVID-19 pandemics is its basic reproduction number, estimations for which were provided in numerous early studies; see Refs within [3]. The basic reproduction number, R_0 , is the average number of secondary infections produced by an infectious individual in a population where everyone is considered susceptible [4, 5]. Being dependent on human behavior and the biological characteristics of the pathogen, R_0 provides an estimation of the contagiousness of the infectious disease [4] and serves as a threshold parameter; when $R_0 > 1$ the infected increase exponentially, leading to a disease outbreak, while when $R_0 < 1$ the disease spread dies out [4, 5].

For the control of the COVID-19 outbreak, various interventions are employed aiming to “flatten” the curve of the epidemics. Since R_0 is constant in time, it cannot monitor the effect of the undertaken measures; instead, the time-varying *effective* reproduction number R_t is utilized, that estimates the secondary infections produced by an infectious individual during the course of an outbreak, thus, in a population where not everyone is considered susceptible. As a result, during the evolution of the epidemics, the undertaken control measures affect R_t , since they influence (i) the duration of contagiousness, (ii) the likelihood of infection per contact and (iii) the contact rate of the infection [4, 6]. The impact of various interventions (case isolation,

*Corresponding author

Email address: dpatsatzis@mail.ntua.gr (Dimitris G. Patsatzis)

contact tracing, travel restrictions, etc.) in R_t has been assessed in a number of studies to provide guidelines in decision-making policies [7–12].

The use of R_0 as a threshold parameter is related to the stability of the disease-free equilibrium (DFE) of the epidemiological model under consideration [4, 5, 13], which is locally assessed by the existence of positive eigenvalues. During the evolution of the system, the local dynamics is characterized by timescales of dissipative/explosive nature - associated with positive/negative eigenvalues - the action of which tends to drive the system towards to/away from equilibrium [14, 15]. Timescale analysis has been frequently employed to address the dynamical properties of systems arising from reactive flows [16, 17], systems biology [18, 19], pharmacokinetics [20], etc, but, to my knowledge, it hasn't been widely applied to population dynamics.

Motivated by the fact that R_0 mathematically expresses the stability of the DFE; i.e., the existence of positive eigenvalues at day zero, here the relation of R_t to the explosive timescales (positive eigenvalues) during the course of COVID-19 outbreak in Italy was investigated. It is shown that the existence of an explosive timescale implies $R_t > 1$, while its absence implies $R_t < 1$. In addition, as this timescale converges/diverges with the immediately slowest one, R_t was shown to approaches to/withdraws from its threshold value 1. Finally, by performing the analysis in 4 different population dynamics models, it is demonstrated that timescale analysis is a robust methodology to monitor the progression of the epidemics, since it directly reflects the variations in R_t , without being hindered by the complexity of the selected model.

2. Materials and Methods

Compartmental modeling is widely used for the analysis of various infectious diseases [21–24], among which COVID-19 pandemics [8, 11, 25, 26]. Four population dynamics compartmental models in the framework of the SIR model [27] were analyzed here. The effective reproduction number R_t was calculated on the basis of these models and conclusions were drawn on its relation to the timescales characterizing the dynamics of each model.

The four compartmental models are presented in Section 2.1, followed by the parameter estimation process considered for their calibration against the data of Italy in Section 2.2. The methodology to calculate the effective reproduction number R_t and the timescales τ_i on the basis of each model is presented in Sections 2.3 and 2.4, respectively.

2.1. The population dynamics models

The SIR model formulates the transmission of an infectious disease among three population groups, namely the *susceptible*, *infected* and *recovered* individuals [27]. In this framework, four population dynamics models were considered, the SIRD, SEIRD, SEInSRD and SIDARTHE models, the governing equations of which can be written in the ODE form:

$$\frac{d}{dt}\mathbf{y} = \mathbf{g}(\mathbf{y}) \quad (1)$$

where \mathbf{y} is the N-dim. column *state vector*, which includes the fraction of each population group over the total population and $\mathbf{g}(\mathbf{y})$ is the N-dim. column *vector field*, which incorporates the transition rates from one population group to another.

The simplest compartmental model to capture COVID-19 pandemics is the SIRD model, which essentially is the SIR model with the addition of a compartment accounting for the *dead* individuals. Denoting S , I , R and D the fraction of susceptible, infected, recovered and dead individuals respectively, over the total population N , the SIRD model is written in the form of Eq. (1) as:

$$\frac{d}{dt} \begin{bmatrix} S \\ I \\ R \\ D \end{bmatrix} = \begin{bmatrix} -\beta SI \\ \beta SI - (\gamma + \mu)I \\ \gamma I \\ \mu I \end{bmatrix} \quad (2)$$

where β is the transmission ratio, γ the recovery ratio, which also expresses the inverse of the infection period of the disease, and μ the fatality ratio.

A more realistic assumption for COVID-19 infection is the existence of an incubation (latency) period, during which an individual is infected but yet not infectious [28, 29]. Such an assumption can be incorporated

in the SIRD model with the addition of a compartment accounting for *exposed* individuals. Denoting E their fraction over the total population, the resulting SEIRD model is written in the form of Eq. (1) as:

$$\frac{d}{dt} \begin{bmatrix} S \\ E \\ I \\ R \\ D \end{bmatrix} = \begin{bmatrix} -\beta SI \\ \beta SI - \sigma E \\ \sigma E - (\gamma + \mu)I \\ \gamma I \\ \mu I \end{bmatrix} \quad (3)$$

where σ is the transition ratio from exposed to infected individuals, expressing the inverse of the incubation period of the disease.

In addition, it has been shown that the COVID-19 infected individuals have symptoms of different severity, varying from mild to severe [30]. Since the severely infected individuals are in need of immediate health care, a more biologically realistic assumption for COVID-19 infection is the distinction between *normally infected* and *severely infected* individuals. Such an assumption can be incorporated in the SEIRD model, by dividing the infected compartment in two sub-compartments. Denoting IN and IS the fraction of normally and severely infected individuals over the total population, the resulting SEInsRD model in the form of Eq. (1) reads:

$$\frac{d}{dt} \begin{bmatrix} S \\ E \\ IN \\ IS \\ R \\ D \end{bmatrix} = \begin{bmatrix} -\beta_N S.IN - \beta_S S.IS - \mu_{TP} S \\ \beta_N S.IN + \beta_S S.IS - \sigma E - \mu_{TP} E \\ (1 - ss)\sigma E - \gamma IN - \mu_N IN \\ ss\sigma E - \gamma IS - \mu_S IS \\ \gamma(IN + IS) - \mu_{TP} R \\ \mu_N IN + \mu_S IS \end{bmatrix} \quad (4)$$

where the subscripts N and S indicate the normally and severely infected transmission β and fatality μ ratios, ss denotes the fraction of severely over normally infected individuals and μ_{TP} is the physiological death ratio.

Finally, a more detailed compartmental model was considered, accounting for susceptible (S), asymptomatic detected and undetected infected (I and D), symptomatic detected and undetected infected (A and R), severely symptomatic (T), healed (H) and extinct (E) individuals, namely the SIDARTHE model [25]. Here, the SIDARTHE model was considered for validation purposes and thus, only a brief description of the model is provided in Appendix A; details can be found in [25]. Note that the SIDARTHE model is also written in the form of Eq. (1); see Eq. (A.13) and Eqs. (1-8) in *Methods* section in [25].

2.2. Model calibration

In this study only the SEIRD and SEInsRD models in Eqs. (3, 4) respectively, were calibrated, since (i) the relation of R_t with the timescales can be reached analytically on the basis of the SIRD model in Eq. (2) and (ii) the parameter values of the SIDARTHE model are provided in [25].

The SEIRD and SEInsRD models in Eqs. (3, 4) were calibrated to the daily reported data of infected, recovered and dead individuals in Italy, as reported by John Hopkins database [31]. The parameter estimation process was performed in a weekly basis accounting for the data from February 26 (week 0) to September 30 (week 30). February 26 was selected as starting day in order to minimize early data distortion, since more than 400 infected individuals were reported at that date. Initially, given the reported fraction of infected, recovered and dead population groups at week 0 - and the susceptible one, through conservation of the total population - the fraction of the exposed, normally infected and severely infected population groups was estimated. In the following, a parameter estimation process was performed in a weekly basis, given these 3 reported data sets, through a genetic algorithm provided by the open-source COPASI software [32, 33]. The initial conditions at day 0 of each week were the predicted values at day 7 of the previous week, in order to preserve continuity in the solution. The resulting parameter sets are depicted for SEIRD and SEInsRD models in Fig. B.1 of Appendix B.

A schematic representation of the SEIRD and SEInsRD models is provided in the left panels of Figs. 1 and 2, respectively. The profiles of infected, recovered and dead individuals, resulted from the aforementioned parameter estimation process, are in very good agreement with the reported data, as shown in the middle panels of Figs. 1 and 2 for the SEIRD and SEInsRD models, respectively. Note that in the case of SEInsRD

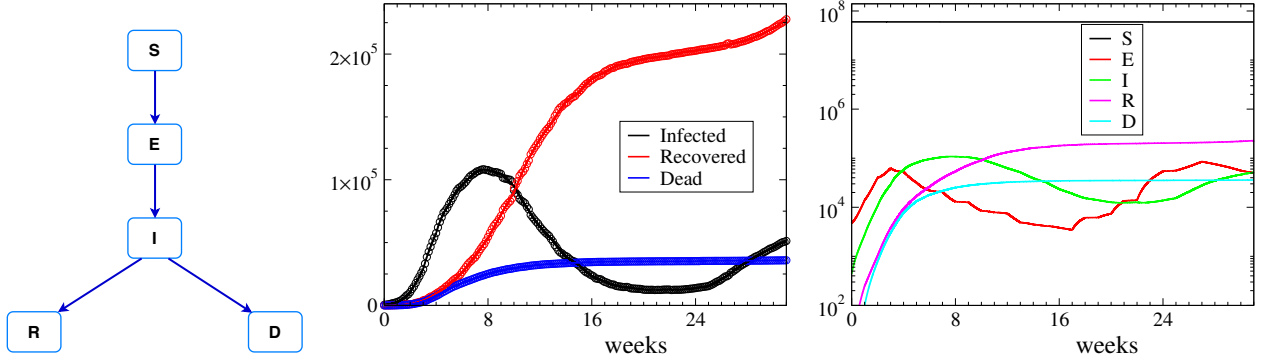


Figure 1: The SEIRD model (left), its fitting against the reported data for Italy in circles (middle) and the profiles of all the population groups (right). The parameter estimation process was performed in a weekly basis from the 26th of February (week 0) to the 30th of September (week 30), accounting for the reported data of infected, recovered and dead individuals.

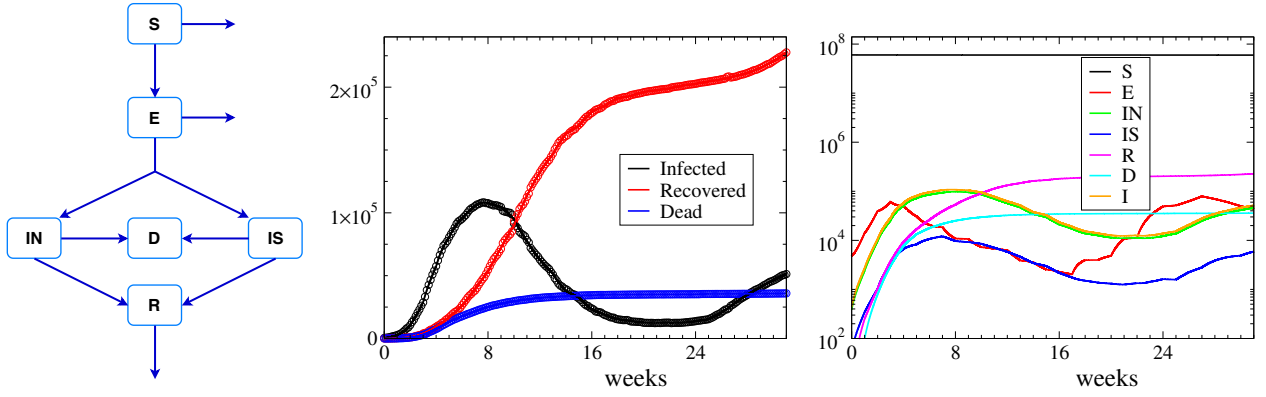


Figure 2: The SEInsRD model (left), its fitting against the reported data for Italy in circles (middle) and the profiles of all the population groups (right). The parameter estimation process was performed in a weekly basis from the 26th of February (week 0) to the 30th of September (week 30), accounting for the reported data of infected, recovered and dead individuals.

model, the sum of the normally and severely infected individuals $I = IN + IS$ was fitted against the reported data set of the infected individuals. The very good agreement of the model parameters to the reported data can be also demonstrated by the R^2 values of both fittings shown in Table B.1 of Appendix B, combined with the respective p-values, which in all cases are $p \ll 0.05$. Finally, the profiles of all the population groups are displayed in the right panels of Figs. 1 and 2, in which great agreement of the population profiles between the two models is reported.

Finally, the SIDARTHE model parameters were directly adopted by [25], following a slightly different approach than the one followed here for SEIRD and SEInsRD models. First, due to availability of data, here the SEIRD and SEInsRD models were calibrated for Italy from February 26 to September 30, while the SIDARTHE model was calibrated for Italy from February 20 to April 5. Second, here the SEIRD and SEInsRD models were calibrated in a constant, 7-days long, time frame, while the SIDARTHE model was calibrated in varying time frames, depending on the interventions undertaken in Italy [25]. Last but not least, the reported data of infected, recovered and dead individuals were considered in our analysis, while in [25] only the ones of infected and recovered (not fitted to the *healed* compartment of the model) individuals.

2.3. Estimation of the reproduction number

The basic reproduction number, R_0 , is a constant biological parameter that provides an estimation of the contagiousness of the infectious disease. It also serves as a threshold parameter; when $R_0 > 1$, one infected individual can trigger an outbreak, while when $R_0 < 1$, the infection will not spread in the population [4, 5].

When various non-pharmaceutical interventions (NPI) are in place, the effective reproduction number R_t is utilized, instead of R_0 , to monitor the reproduction number during the evolution of the outbreak. R_t

provides an estimation of the contagiousness of the infectious disease, during the course of an outbreak, where not every individual is considered susceptible. Considering that all model parameters are time dependant, we estimated R_t for COVID-19 pandemics in Italy using the Next Generation Matrix (NGM) approach [13, 34, 35], which yields in the following expressions for the SIRD, SEIRD, SEInsRD and SIDARTHE models:

$$\begin{aligned} R_t^{SIRD} &= \frac{\beta}{\gamma + \mu} = R_t^{SEIRD} \\ R_t^{SEInsRD} &= \frac{\sigma}{\sigma + \mu_{TP}} \left(\frac{(1 - ss)\beta_N}{\gamma + \mu_N} + \frac{ss\beta_S}{\gamma + \mu_S} \right) \\ R_t^{SIDARTHE} &= \frac{\alpha}{r_1} + \frac{\beta\epsilon}{r_1 r_2} + \frac{\gamma\zeta}{r_1 r_3} + \frac{\delta\theta\zeta}{r_1 r_3 r_4} + \frac{\delta\epsilon\eta}{r_1 r_2 r_4} \end{aligned} \quad (5)$$

where $\alpha, \beta, \gamma, \delta, \epsilon, \zeta, \eta, \theta$ are model parameters of the SIDARTHE model and $r_1 = \epsilon + \lambda + \zeta$, $r_2 = \eta + \rho$, $r_3 = \kappa + \mu + \theta$ and $r_4 = \nu + \xi$. Note that the expression of R_t for SIDARTHE model estimated here via the NGM approach is the same with the one derived in [25].

A brief discussion on NGM approach is provided in Appendix A, along with details on the calculation of R_t on the basis of the four population dynamics models.

2.4. Calculation of the time scales

Given a system of ODEs in the matrix form of Eq. (1), the timescales are calculated as the inverse modulus of the eigenvalues of the $N \times N$ Jacobian matrix $\mathbf{J}(\mathbf{y}) = \nabla_{\mathbf{y}}(\mathbf{g}(\mathbf{y}))$ [14, 15]. The timescales are of dissipative/explosive nature, i.e., the components of the system that generate them tend to drive the system towards to/away from equilibrium, when the respective eigenvalue has negative/positive real part.

When a complex mathematical model in the form of Eq. (1) is encountered, it is usually impossible to calculate analytic expressions for its eigenvalues and thus its timescales. This is the case of the SEIRD, SEInsRD and SIDARTHE models, for which the timescales were calculated numerically. However, in the case of the SIRD model, the non-zero eigenvalues can be calculated analytically as:

$$\lambda_{1,2} = \frac{1}{2} \left(X \pm \sqrt{X^2 - 4Y} \right) \quad X = -\gamma - \beta I - \mu + \beta S \quad Y = \beta I(\gamma + \mu) \quad (6)$$

Therefore, the related timescales are of explosive nature (either real or complex $\lambda_{1,2}$) if and only if:

$$X > 0 \Rightarrow \beta(S - I) > \gamma + \mu \Rightarrow \frac{\beta(S - I)}{\gamma + \mu} > 1 \quad (7)$$

Equation (7) provides the condition under which the explosive timescales of the SIRD model arise, a feature that will be associated in the following section with R_t .

3. Results

The impact of the undertaken NPIs in COVID-19 pandemics is assessed by the effect that they introduce in the reproduction number [7–12]. Here, we show that the insights provided by the utilization of the effective reproduction number R_t during the progression of the COVID-19 pandemics can be deduced by timescale analysis. In particular, it is shown that:

- i) the existence of an explosive timescale during the progression of COVID-19 epidemics implies $R_t > 1$, while its absence implies $R_t < 1$, and
- ii) the tendency of this timescale to converge/diverge with the immediately slowest one, implies that R_t tends to approach to/withdraw from its threshold value 1.

These results are reached on the basis of the four population dynamics models discussed in Section 2.1, for the case of Italy.

3.1. The explosive timescales in relation to the reproduction number

The first indication on the relation of the explosive timescales to the reproduction number is provided by the analysis of the SIRD model in Eq. (2), that is the simplest model to describe the progression of COVID-19 epidemics. In contrast to more complicated models, the timescales of the SIRD model can be calculated analytically. According to Section 2.4, the evolution of the SIRD model is characterized by the action of two timescales $\tau_{1,2} = 1/|\lambda_{1,2}|$; the expressions of $\lambda_{1,2}$ were derived in Eq. (6). Both $\tau_{1,2}$ are of explosive/dissipative nature when the condition in Eq. (7) holds/is violated. Given the expression of R_t for SIRD model in Eq. (5) and that $S - I < S(0) = 1$, Eq. (7) yields:

$$Re(\lambda_{1,2}) > 0 \Leftrightarrow X > 0 \Leftrightarrow \frac{\beta(S - I)}{\gamma + \mu} > 1 \Rightarrow \frac{\beta S(0)}{\gamma + \mu} > 1 \Rightarrow R_t > 1 \quad (8)$$

Equation (8) shows that the existence of explosive timescales implies $R_t > 1$, while their absence implies $R_t < 1$. Note that this outcome, holds true not only for COVID-19 pandemics, but also for any infectious disease, since it was derived by analytical means on the basis of the SIRD model.

Next, the relation of the explosive timescales with R_t was examined using reported data for COVID-19 pandemics in Italy. The SEIRD model in Eq. (3) was adopted and fitted against the reported data sets of infected, recovered and dead individuals in Italy from February 26 to September 30. In order to account for the NPIs undertaken, the SEIRD model was calibrated in a weekly basis following the parameter estimation process described in detail in Section 2.2. The resulting solution is in great agreement with the reported data, as shown in Fig. 1.

The timescales and R_t , estimated on the basis of the SEIRD model in Eq. (5), are displayed in Fig. 3 from week 0 (starting in Feb. 26) to week 30 (ending in Sep. 30). As shown in the left panel of Fig. 3, the evolution of the SEIRD model is characterized by three timescales $\tau_{1,2,3}$, the fastest of which, τ_1 , is always dissipative in nature, while $\tau_{2,3}$ are either dissipative or explosive. In particular, during weeks 0-6 and 20-26, $\tau_{2,3}$ are explosive, as indicated by the shaded background in Fig. 3. The values of R_t are depicted in the right panel of Fig. 3, in which the red dashed horizontal line indicates the threshold value $R_t = 1$. As indicated by the shaded background, the time periods when the explosive nature of timescales $\tau_{2,3}$ is reported coincides with the ones that $R_t > 1$ (weeks 0-6 and 20-26). In contrast, when $\tau_{2,3}$ are of dissipative nature, $R_t < 1$ (weeks 7-19, 27-30). Note that the transition from the explosive to the dissipative nature of the timescales $\tau_{2,3}$, and vice-versa, is immediate, since model calibration is performed in a weekly basis.

Comparison of the explosive timescales and R_t in Fig. 3 reveals the following trend: as the gap between τ_2 and τ_3 decreases/increases, R_t approaches to/withdraws from its threshold value unity. This is particularly clear during the first wave of COVID-19 pandemics in Italy (weeks 0-12). During weeks 0-6, where τ_2 and τ_3 are explosive, their gap tends to decrease, so that R_t decreases, approaching close to unity values. At week 7, τ_2 and τ_3 become dissipative and R_t attains values below 1. From this point on and up to week 12, the gap of τ_2 and τ_3 increases, so that R_t continues to decrease, this time withdrawing from its threshold 1. This behaviour is additionally supported by the fact that during weeks 4-8, 17, 19, 21 and 30, in which R_t

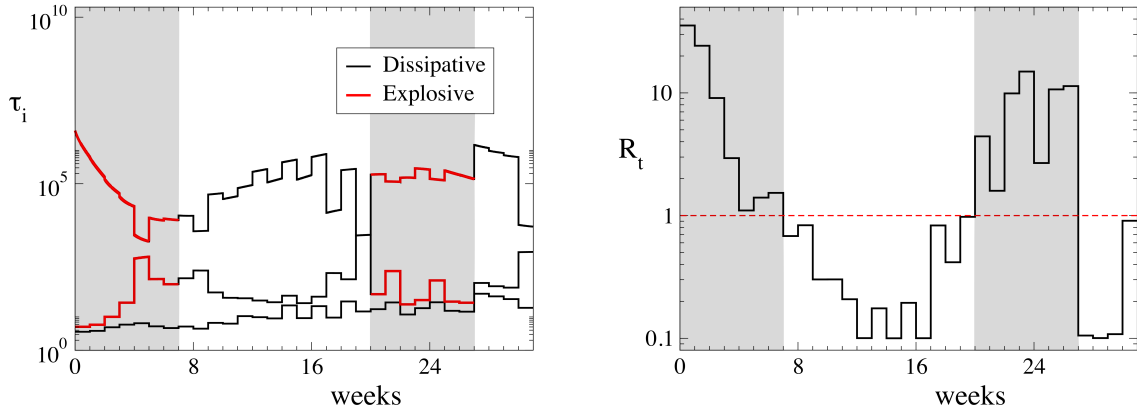


Figure 3: The timescales (left) and the effective reproduction number R_t (right) estimated on the basis of the solution of the SEIRD model shown in Fig. 1.

attains close to 1 values, the gap between τ_2 and τ_3 is small; to the point where $\tau_2 = \tau_3$ in week 19, in which $R_t = 0.96$.

3.2. Robustness

In order to demonstrate the robustness of the relation of the explosive timescales to the reproduction number, a more complicated population dynamics model was considered, the SEInsRD model. The SEInsRD model in Eq. (4) was adopted and calibrated to the same reported data sets with SEIRD model in Section 3.1, corresponding to infected, recovered and dead individuals in Italy from February 26 to September 30. Similarly to SEIRD model, the SEInsRD model calibration was performed in a weekly basis following the process described in Section 2.2 and the resulting solution is in great agreement with the reported data, as shown in Fig. 2.

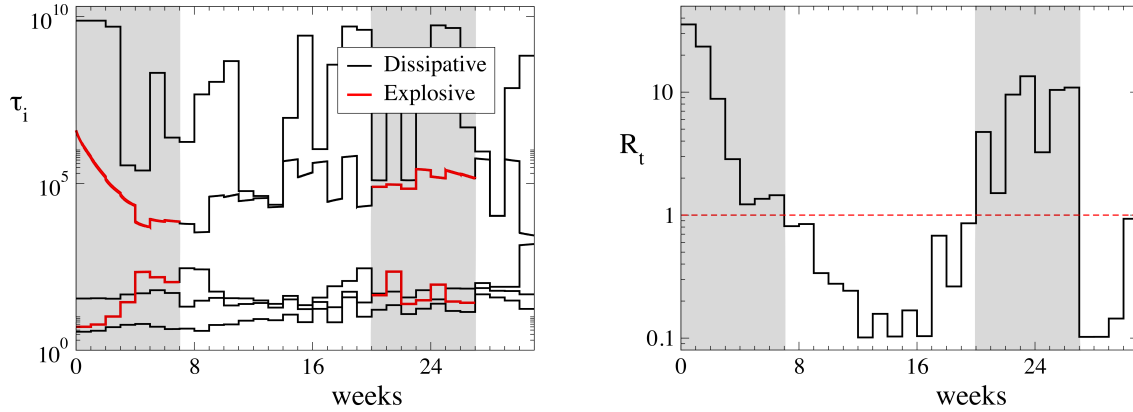


Figure 4: The timescales (left) and the reproduction number R_t (right) calculated on the basis of the solution of the SEInsRD model shown in Fig. 2.

The timescales and R_t , estimated on the basis of the SEInsRD model in Eq. (5), are displayed in Fig. 4 from week 0 (starting in Feb. 26) to week 30 (ending in Sep. 30). As shown in the left panel of Fig. 4, the evolution of SEInsRD model is characterized by 5 timescales: three of which are always of dissipative nature and the remaining ones are either explosive or dissipative; denoting $\tau_{exp,f}$ the fast explosive timescale and $\tau_{exp,s}$ the slow one. In particular, during weeks 0-6 and 20-26, $\tau_{exp,f}$ and $\tau_{exp,s}$ are explosive, as indicated by the shaded background in Fig. 4. The right panel of Fig. 4 displays the values of R_t in comparison to the threshold value $R_t = 1$ indicated by the red dashed horizontal line. Similarly to the SEIRD model, it is shown by the shaded background that $R_t > 1$ when the $\tau_{exp,f}$ and $\tau_{exp,s}$ are explosive (weeks 0-6 and 20-26), while $R_t < 1$ when they lose this character and become dissipative (weeks 7-19 and 27-30). In addition, the trend of increasing/decreasing gap of $\tau_{exp,f}$ and $\tau_{exp,s}$ is again reflected in R_t approaching to/withdrawing from its threshold value 1. In particular, it is shown that the closer the values of R_t to 1, (weeks 4-8, 17, 19, 21 and 30), the smaller the gap between $\tau_{exp,f}$ and $\tau_{exp,s}$; to the point where $R_t = 0.97$ in week 30, in which $\tau_{exp,f} \approx \tau_{exp,s}$. In summary, the qualitative results on the relation of the explosive timescales to R_t are maintained on the basis of the SEInsRD model.

3.3. Validation

In order to validate the qualitative results, reached on the basis of the SEIRD and SEInsRD models, regarding to the relation of the explosive timescales to R_t , a more complicated SIDARTHE model was considered [25], as briefly discussed in Section 2.1.

The profiles of the population groups accounted for in the SIDARTHE model were reproduced, adopting the model parameters in [25]. On the basis of the SIDARTHE solution, the timescales were calculated and R_t was estimated according to the expression in Eq. (5). The resulting values are displayed in Fig. 5 starting from day -6 (Feb 20) and ending in day 40 (Apr 5); day 0 was chosen to be Feb 26 for comparison with Figs. 3 and 4. As shown in the left panel of Fig. 5, the evolution of SIDARTHE model is characterized by six timescales, four among which are always dissipative in nature, while the remaining two are either dissipative or explosive; denoted as $\tau_{exp,f}$ and $\tau_{exp,s}$. In particular, $\tau_{exp,f}$ and $\tau_{exp,s}$ are explosive from day -6 to day 22,

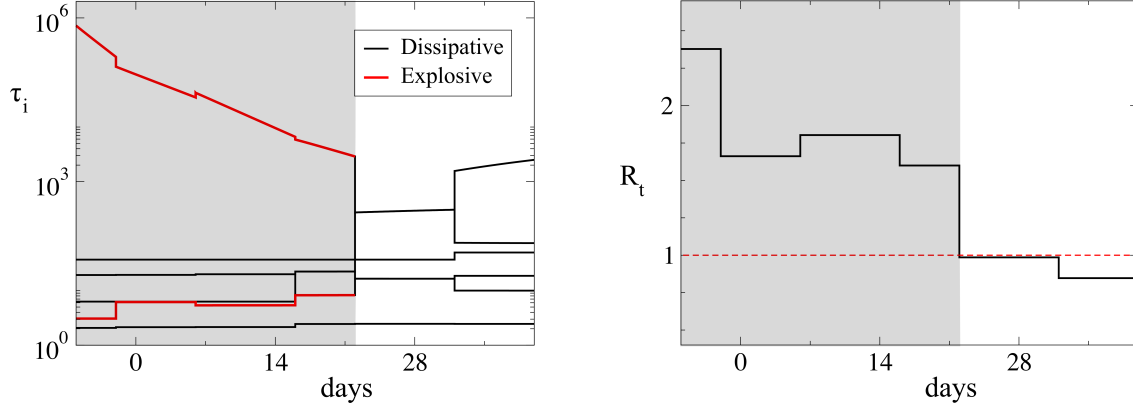


Figure 5: The timescales and reproduction number R_t calculated on the basis of SIDARTHE model, that was calibrated for Italy data in [25].

as indicated by the shaded background in Fig. 5. The values of R_t are depicted in the right panel of Fig. 5, in which the red dashed horizontal line indicates the threshold value $R_t = 1$. As indicated by the shaded background, the explosive nature of timescales $\tau_{exp,f}$ and $\tau_{exp,s}$ implies $R_t > 1$ (days -6-22), while losing such a nature and becoming dissipative, implies $R_t < 1$ (days 23-40). In addition, it is shown that as the gap between $\tau_{exp,f}$ and $\tau_{exp,s}$ becomes smaller, R_t approaches its threshold value unity, to the point when $R_t = 0.986$ during days 23-33, in which $\tau_{exp,f} = \tau_{exp,s}$.

It should be noted here that, the evolution of timescales $\tau_{exp,f}$ and $\tau_{exp,s}$ and the reproduction number R_t , calculated on the basis of SIDARTHE model, is different in comparison to those calculated on the basis of SEIRD and SEInsRD models. In particular, on the basis of the SIDARTHE model, the timescales are explosive in nature and $R_t > 1$ until to day 22, while on the basis of the SEIRD and SEInsRD models until day 42. Despite this being a major difference, that originates from differences in model calibration as discussed in Section 2.2, the relation of the explosive timescales to R_t , deduced on the basis of SEIRD and SEInsRD models, is validated by the analysis with the SIDARTHE model.

4. Conclusions

The progression of an infectious disease spread like COVID-19 pandemics is frequently examined by population dynamics models [8, 11, 21–26]. Their evolution as dynamical systems is characterized by timescales that are either of dissipative or explosive nature; i.e., their action tends to drive the system either towards to or away from equilibrium [14, 15]. The basic reproduction number R_0 as a threshold parameter provides such an intuition, in the view that when $R_0 < 1$ the system is driven towards to its DFE, so that the infection does not spread in the population, while when $R_0 > 1$ the system is driven away from its DFE, so that the disease spreads exponentially [4, 5]. In the case of an outbreak, such as COVID-19 pandemics, in which early predictions showed $R_0 \approx 2 - 3$ [3], various NPIs are employed during the evolution of the outbreak, aiming to “flatten” the curve of the epidemics. The influence of the NPIs is frequently assessed by the reduction that they introduce to the effective reproduction number R_t , [7–12]; ideally making $R_t < 1$, which indicates that the disease spread will eventually die out. In this work, the relation of the effective reproduction number R_t with the timescales characterizing the evolution of the epidemic spread was examined in the case of COVID-19 pandemics in Italy from February 26 to September 30.

In particular, it was demonstrated analytically on the basis of the SIRD model and numerically on the basis of the SEIRD model in Section 3.1, that when two of the timescales characterizing the evolution of the epidemic spread are of explosive nature, the effective reproduction number is above its threshold value; i.e., $R_t > 1$. On the contrary, when all the timescales are of dissipative nature it is implied that $R_t < 1$. In addition, the following trending behaviour was revealed: as the gap between the two explosive timescales increases/decreases, R_t approaches to/withdraws from its threshold value 1, as shown in Fig. 3. These outcomes suggest that the insights provided by the utilization of R_t as a threshold parameter can be also obtained by timescale analysis.

This work additionally suggests that timescale analysis is a robust methodology to assess the progression of the epidemic spread, since it is not hindered by the complexity of the selected model, nor the calibration process followed to fit the model against the reported data. Following the same model calibration procedure to the SEInsRD model, resulted in timescales that are almost equal to the ones of the SEIRD model; see Figs. 3 and 4. Such a result indicates that the relation of the explosive timescales to R_t is not affected by model selection, as discussed in Section 3.2. In addition, this relation is not affected by the parameter estimation process either, as demonstrated through the analysis of the SIDARTHE model, the calibration of which in [25] had significant differences with the one followed here for SEIRD and SEInsRD models; see Section 2.2.

In conclusion, timescale analysis is a rigorous mathematical methodology to assess the progression of an epidemic spread, since it can effectively provide the insight obtained by the reproduction number. Timescale analysis is not hindered by model selection in contrast to the reproduction number that is highly dependable on the structure of the selected model [4]. In addition, the expression of the reproduction number becomes more complex as the detail of the model increases, as shown in Eq. (5); compare for example R_t for SEIRD and SIDARTHE models. In contrast, timescale analysis can be performed in an algorithmic fashion, utilizing the diagnostic tools of *Computational Singular Perturbation* [14, 36] that have been effectively employed to address the dynamical properties of systems arising from a wide variety of fields [16–20]. More importantly, the use of timescale analysis for the assessment of various NPIs is promising, since it can determine via its algorithmic tools the factors that play the most significant role on the control of ongoing COVID-19 outbreak.

5. Acknowledgements

This publication is based upon work supported by the Khalifa University of Science and Technology, under Award No. CPRA-2020-Goussis.

References

- [1] World Health Organization. WHO Director-General’s opening remarks at the media briefing on COVID-19, March 11, 2020, <https://www.who.int/dg/speeches/detail/who-director-general-s-opening-remarks-at-the-media-briefing-on-covid-19\0T1\textemdash11-march-2020>, accessed: 2020-03-11.
- [2] Worldometer. COVID-19 Coronavirus Pandemic, <https://www.worldometers.info/coronavirus/>, accessed: 2021-1-15.
- [3] Y. Liu, A. A. Gayle, A. Wilder-Smith, J. Rocklöv, The reproductive number of covid-19 is higher compared to sars coronavirus, *Journal of travel medicine*.
- [4] P. L. Delamater, E. J. Street, T. F. Leslie, Y. T. Yang, K. H. Jacobsen, Complexity of the basic reproduction number (r_0), *Emerging infectious diseases* 25 (1) (2019) 1.
- [5] O. Diekmann, J. A. P. Heesterbeek, J. A. Metz, On the definition and the computation of the basic reproduction ratio r_0 in models for infectious diseases in heterogeneous populations, *Journal of mathematical biology* 28 (4) (1990) 365–382.
- [6] G. Viceconte, N. Petrosillo, Covid-19 r_0 : Magic number or conundrum?, *Infectious disease reports* 12 (1).
- [7] J. Hellewell, S. Abbott, A. Gimma, N. I. Bosse, C. I. Jarvis, T. W. Russell, J. D. Munday, A. J. Kucharski, W. J. Edmunds, F. Sun, et al., Feasibility of controlling covid-19 outbreaks by isolation of cases and contacts, *The Lancet Global Health*.
- [8] A. J. Kucharski, T. W. Russell, C. Diamond, Y. Liu, J. Edmunds, S. Funk, R. M. Eggo, F. Sun, M. Jit, J. D. Munday, et al., Early dynamics of transmission and control of covid-19: a mathematical modelling study, *The lancet infectious diseases*.
- [9] A. Pan, L. Liu, C. Wang, H. Guo, X. Hao, Q. Wang, J. Huang, N. He, H. Yu, X. Lin, et al., Association of public health interventions with the epidemiology of the covid-19 outbreak in wuhan, china, *Jama* 323 (19) (2020) 1915–1923.

- [10] B. J. Cowling, S. T. Ali, T. W. Ng, T. K. Tsang, J. C. Li, M. W. Fong, Q. Liao, M. Y. Kwan, S. L. Lee, S. S. Chiu, et al., Impact assessment of non-pharmaceutical interventions against coronavirus disease 2019 and influenza in hong kong: an observational study, *The Lancet Public Health*.
- [11] B. Tang, X. Wang, Q. Li, N. L. Bragazzi, S. Tang, Y. Xiao, J. Wu, Estimation of the transmission risk of the 2019-ncov and its implication for public health interventions, *Journal of clinical medicine* 9 (2) (2020) 462.
- [12] B. Tang, N. L. Bragazzi, Q. Li, S. Tang, Y. Xiao, J. Wu, An updated estimation of the risk of transmission of the novel coronavirus (2019-ncov), *Infectious disease modelling* 5 (2020) 248–255.
- [13] P. Van den Driessche, J. Watmough, Reproduction numbers and sub-threshold endemic equilibria for compartmental models of disease transmission, *Mathematical biosciences* 180 (1-2) (2002) 29–48.
- [14] S. Lam, D. Goussis, Understanding complex chemical kinetics with computational singular perturbation, in: *Symposium (International) on Combustion*, Vol. 22, Elsevier, 1989, pp. 931–941.
- [15] U. Maas, S. B. Pope, Simplifying chemical kinetics: intrinsic low-dimensional manifolds in composition space, *Combustion and flame* 88 (3-4) (1992) 239–264.
- [16] D. M. Manias, E. A. Tingas, C. E. Frouzakis, K. Boulouchos, D. A. Goussis, The mechanism by which ch_2o and h_2o_2 additives affect the autoignition of ch_4/air mixtures, *Combustion and Flame* 164 (2016) 111–125.
- [17] E. A. Tingas, D. C. Kyritsis, D. A. Goussis, Autoignition dynamics of dme/air and etoh/air homogeneous mixtures, *Combustion and Flame* 162 (9) (2015) 3263–3276.
- [18] P. D. Kourdis, R. Steuer, D. A. Goussis, Physical understanding of complex multiscale biochemical models via algorithmic simplification: Glycolysis in *saccharomyces cerevisiae*, *Physica D: Nonlinear Phenomena* 239 (18) (2010) 1798–1817.
- [19] D. G. Patsatzis, D. A. Goussis, A new michaelis-menten equation valid everywhere multi-scale dynamics prevails, *Mathematical biosciences* 315 (2019) 108220.
- [20] D. G. Patsatzis, D. T. Maris, D. A. Goussis, Asymptotic analysis of a target-mediated drug disposition model: algorithmic and traditional approaches, *Bulletin of mathematical biology* 78 (6) (2016) 1121–1161.
- [21] S. Gao, L. Chen, Z. Teng, Pulse vaccination of an seir epidemic model with time delay, *Nonlinear Analysis: Real World Applications* 9 (2) (2008) 599–607.
- [22] L. Canini, F. Carrat, Population modeling of influenza a/h1n1 virus kinetics and symptom dynamics, *Journal of virology* 85 (6) (2011) 2764–2770.
- [23] L. Esteva, C. Vargas, Coexistence of different serotypes of dengue virus, *Journal of mathematical biology* 46 (1) (2003) 31–47.
- [24] A. Stegeman, A. R. Elbers, J. Smak, M. C. de Jong, Quantification of the transmission of classical swine fever virus between herds during the 1997–1998 epidemic in the netherlands, *Preventive veterinary medicine* 42 (3-4) (1999) 219–234.
- [25] G. Giordano, F. Blanchini, R. Bruno, P. Colaneri, A. Di Filippo, A. Di Matteo, M. Colaneri, Modelling the covid-19 epidemic and implementation of population-wide interventions in italy, *Nature Medicine* (2020) 1–6.
- [26] L. Russo, C. Anastassopoulou, A. Tsakris, G. N. Bifulco, E. F. Campana, G. Toraldo, C. Siettos, Tracing day-zero and forecasting the fade out of the covid-19 outbreak in lombardy, italy: A compartmental modelling and numerical optimization approach., *medRxiv*.

- [27] W. O. Kermack, A. G. McKendrick, A contribution to the mathematical theory of epidemics, Proceedings of the royal society of london. Series A, Containing papers of a mathematical and physical character 115 (772) (1927) 700–721.
- [28] S. A. Lauer, K. H. Grantz, Q. Bi, F. K. Jones, Q. Zheng, H. R. Meredith, A. S. Azman, N. G. Reich, J. Lessler, The incubation period of coronavirus disease 2019 (covid-19) from publicly reported confirmed cases: estimation and application, Annals of internal medicine 172 (9) (2020) 577–582.
- [29] Q. Li, X. Guan, P. Wu, X. Wang, L. Zhou, Y. Tong, R. Ren, K. S. Leung, E. H. Lau, J. Y. Wong, et al., Early transmission dynamics in wuhan, china, of novel coronavirus–infected pneumonia, New England Journal of Medicine.
- [30] V. Surveillances, The epidemiological characteristics of an outbreak of 2019 novel coronavirus diseases (covid-19)—china, 2020, China CDC Weekly 2 (8) (2020) 113–122.
- [31] COVID-19 Data Repositoy by the Center for Systems Science and Engineering (CSSE) at Johns Hopkins University, <https://github.com/CSSEGISandData/COVID-19>, accessed: 2020-06-26.
- [32] T. P. Runarsson, X. Yao, Stochastic ranking for constrained evolutionary optimization, IEEE Transactions on evolutionary computation 4 (3) (2000) 284–294.
- [33] S. Hoops, S. Sahle, R. Gauges, C. Lee, J. Pahle, N. Simus, M. Singhal, L. Xu, P. Mendes, U. Kummer, Copasi—a complex pathway simulator, Bioinformatics 22 (24) (2006) 3067–3074.
- [34] J. M. Heffernan, R. J. Smith, L. M. Wahl, Perspectives on the basic reproductive ratio, Journal of the Royal Society Interface 2 (4) (2005) 281–293.
- [35] P. van den Driessche, Reproduction numbers of infectious disease models, Infectious Disease Modelling 2 (3) (2017) 288–303.
- [36] S. Lam, D. Goussis, The csp method for simplifying kinetics, International journal of chemical kinetics 26 (4) (1994) 461–486.

Appendix A. Derivation of the effective reproduction number

The Next Generation Matrix (NGM) approach is utilized for the calculation of the basic reproduction number R_0 [13, 34, 35]. Given a system of ODEs in the form of Eq. (1), let y_j be the $j = 1, \dots, m$ infected population groups among all the y_i populations groups of the $i = 1, \dots, n$ compartments in \mathbf{y} . In turn, let $F_i(\mathbf{y})$ be the rate of appearance of new infections in the i -th compartment and $V_i(\mathbf{y}) = V_i^-(\mathbf{y}) - V_i^+(\mathbf{y})$ the transition rates out of (V^-) and into (V^+) the i -th compartment. By definition, it is implied that:

$$\frac{dy_i}{dt} = F_i(\mathbf{y}) - V_i(\mathbf{y}) = F_i(\mathbf{y}) + V_i^+(\mathbf{y}) - V_i^-(\mathbf{y}) \quad (\text{A.1})$$

Let the matrices \mathbf{F} and \mathbf{V} be:

$$\mathbf{F} = \left[\frac{\partial F_i(\mathbf{y}^*)}{\partial y_j} \right] \quad \text{and} \quad \mathbf{V} = \left[\frac{\partial V_i(\mathbf{y}^*)}{\partial y_j} \right] \quad (\text{A.2})$$

where \mathbf{y}^* is the disease-free equilibrium and $i, j = 1, \dots, m$. According to the NGM approach, the basic reproduction number R_0 is the spectral radius (largest eigenvalue) of the matrix $\mathbf{F} \cdot \mathbf{V}^{-1}$; i.e., $R_0 = \rho(\mathbf{F} \cdot \mathbf{V}^{-1})$ [13, 34, 35]. However, since the model parameters vary in time (different parameter values in each week), the NGM approach utilization results in the calculation of the effective reproduction number R_t . In the following, the analytical expressions of R_t for SIRD, SEIRD, SEInsRD and SIDARTHE models in Eq. (5) are derived.

The SIRD mathematical model in Eq. (2) can be written in the form of Eq. (A.1) as:

$$\frac{d}{dt} \begin{bmatrix} S \\ I \\ R \\ D \end{bmatrix} = \begin{bmatrix} 0 \\ \beta SI \\ 0 \\ 0 \end{bmatrix} + \begin{bmatrix} 0 \\ 0 \\ \gamma I \\ \mu I \end{bmatrix} - \begin{bmatrix} \beta SI \\ (\gamma + \mu)I \\ 0 \\ 0 \end{bmatrix} = F_i(\mathbf{y}) + V_i^+(\mathbf{y}) - V_i^-(\mathbf{y}) \quad (\text{A.3})$$

The disease-free equilibrium is $\mathbf{y}^* = (S(0), 0, 0, 0)$, so that substitution in Eq. (A.2) leads to:

$$\mathbf{F} = \beta S(0) \quad \text{and} \quad \mathbf{V} = \gamma + \mu \quad (\text{A.4})$$

Given that $S(0) = 1$ as fraction of the total population, the effective reproduction number for the SIRD model is:

$$R_t = \rho(\mathbf{F} \cdot \mathbf{V}^{-1}) = \frac{\beta}{\gamma + \mu} \quad (\text{A.5})$$

The SEIRD mathematical model in Eq. (3) can be written in the form of Eq. (A.1) as:

$$\frac{d}{dt} \begin{bmatrix} S \\ E \\ I \\ R \\ D \end{bmatrix} = \begin{bmatrix} 0 \\ \beta SI \\ 0 \\ 0 \\ 0 \end{bmatrix} + \begin{bmatrix} 0 \\ 0 \\ \sigma E \\ \gamma I \\ \mu I \end{bmatrix} - \begin{bmatrix} \beta SI \\ \sigma E \\ \gamma I + \mu I \\ 0 \\ 0 \end{bmatrix} = F_i(\mathbf{y}) + V_i^+(\mathbf{y}) - V_i^-(\mathbf{y}) \quad (\text{A.6})$$

The disease-free equilibrium is $\mathbf{y}^* = (S(0), 0, 0, 0, 0)$, so that substitution in Eq. (A.2) leads to:

$$\mathbf{F} = \begin{bmatrix} 0 & \beta S(0) \\ 0 & 0 \end{bmatrix} \quad \text{and} \quad \mathbf{V} = \begin{bmatrix} \sigma & 0 \\ -\sigma & \gamma + \mu \end{bmatrix} \quad (\text{A.7})$$

Given that $S(0) = 1$, the effective reproduction number for the SEIRD model is:

$$R_t = \rho(\mathbf{F} \cdot \mathbf{V}^{-1}) = \frac{\beta}{\gamma + \mu} \quad (\text{A.8})$$

Note that the R_t of SEIRD model is the same to that of SIRD model in Eq. (A.5).

The SEInsRD mathematical model in Eq. (4) can be written in the form of Eq. (A.1) as:

$$\frac{d}{dt} \begin{bmatrix} S \\ E \\ IN \\ IS \\ R \\ D \end{bmatrix} = \begin{bmatrix} 0 \\ \beta_N S.IN + \beta_S S.IS \\ 0 \\ 0 \\ 0 \\ 0 \end{bmatrix} + \begin{bmatrix} 0 \\ 0 \\ (1 - ss)\sigma E \\ ss\sigma E \\ \gamma(IN + IS) \\ \mu_N IN + \mu_S IS \end{bmatrix} - \begin{bmatrix} \beta_N S.IN + \beta_S S.IS + \mu_{TP} S \\ \sigma E + \mu_{TP} E \\ \gamma IN + \mu_N IN \\ \gamma IS + \mu_S IS \\ \mu_{TP} R \\ 0 \end{bmatrix} = F_i(\mathbf{y}) + V_i^+(\mathbf{y}) - V_i^-(\mathbf{y}) \quad (\text{A.9})$$

The disease-free equilibrium is $\mathbf{y}^* = (S(0), 0, 0, 0, 0, 0)$, so that substitution in Eq. (A.2) leads to:

$$\mathbf{F} = \begin{bmatrix} 0 & \beta_N S(0) & \beta_S S(0) \\ 0 & 0 & 0 \\ 0 & 0 & 0 \end{bmatrix} \quad \text{and} \quad \mathbf{V} = \begin{bmatrix} \sigma + \mu_{TP} & 0 & 0 \\ -(1 - ss)\sigma & \gamma + \mu_N & 0 \\ -ss\sigma & 0 & \gamma + \mu_S \end{bmatrix} \quad (\text{A.10})$$

Given that $S(0) = 1$, the effective reproduction number for the SEInsRD model is:

$$R_t = \rho(\mathbf{F} \cdot \mathbf{V}^{-1}) = \frac{\sigma}{\sigma + \mu} \left(\frac{(1 - ss)\beta_N}{\gamma + \mu_N} + \frac{ss\beta_S}{\gamma + \mu_S} \right) \quad (\text{A.11})$$

Note that when considering the $\mu_{TP} \ll \sigma$ limit, R_t of SEInsRD model in Eq. (A.11) is simplified to:

$$R_t \stackrel{\mu_{TP} \ll \sigma}{=} \left(\frac{(1 - ss)\beta_N}{\gamma + \mu_N} + \frac{ss\beta_S}{\gamma + \mu_S} \right) \quad (\text{A.12})$$

which is similar to that of SIRD and SEIRD models in Eqs. (A.5, A.8) when setting $ss = 0$; i.e., when neglecting the severely infected individuals from the model.

Finally, the SIDARTHE mathematical model in [25] can be written in the form of Eq. (A.1) as:

$$\begin{aligned} \frac{d}{dt} \begin{bmatrix} S \\ I \\ D \\ A \\ R \\ T \\ H \\ E \end{bmatrix} &= \begin{bmatrix} -S(\alpha I - \beta D - \gamma A - \delta R) \\ S(\alpha I + \beta D + \gamma A + \delta R) - (\epsilon + \zeta + \lambda)I \\ \epsilon I - (\eta + \rho)D \\ \zeta I - (\theta + \mu + \kappa)A \\ \eta D + \theta A - (\nu + \xi)R \\ \mu A + \nu R - (\sigma + \tau)T \\ \lambda I + \rho D + \kappa A + \xi R + \sigma T \\ \tau T \end{bmatrix} = \begin{bmatrix} 0 \\ S(\alpha I + \beta D + \gamma A + \delta R) \\ 0 \\ 0 \\ 0 \\ 0 \\ 0 \\ 0 \end{bmatrix} + \\ &+ \begin{bmatrix} 0 \\ 0 \\ \epsilon I \\ \zeta I \\ \eta D + \theta A \\ \mu A + \nu R \\ \lambda I + \rho D + \kappa A + \xi R + \sigma T \\ \tau T \end{bmatrix} - \begin{bmatrix} S(\alpha I - \beta D - \gamma A - \delta R) \\ (\epsilon + \zeta + \lambda)I \\ (\eta + \rho)D \\ (\theta + \mu + \kappa)A \\ (\nu + \xi)R \\ (\sigma + \tau)T \\ 0 \\ 0 \end{bmatrix} = F_i(\mathbf{y}) + V_i^+(\mathbf{y}) - V_i^-(\mathbf{y}) \quad (\text{A.13}) \end{aligned}$$

where the parameter notation is explained in detail in [25]. The disease-free equilibrium is $\mathbf{y}^* = (S(0), 0, 0, 0, 0, 0, 0, 0)$, so that substitution in Eq. (A.2) leads to:

$$\mathbf{F} = \begin{bmatrix} \alpha S(0) & \beta S(0) & \gamma S(0) & \delta S(0) & 0 \\ 0 & 0 & 0 & 0 & 0 \\ 0 & 0 & 0 & 0 & 0 \\ 0 & 0 & 0 & 0 & 0 \\ 0 & 0 & 0 & 0 & 0 \end{bmatrix} \quad \text{and} \quad \mathbf{V} = \begin{bmatrix} \epsilon + \lambda + \zeta & 0 & 0 & 0 & 0 \\ -\epsilon & \eta + \rho & 0 & 0 & 0 \\ -\zeta & 0 & \kappa + \mu + \theta & 0 & 0 \\ 0 & -\eta & -\theta & \nu + \xi & 0 \\ 0 & 0 & \mu & \nu & \sigma + \tau \end{bmatrix} \quad (\text{A.14})$$

Given that $S(0) = 1$, the effective reproduction number for the SIDARTHE model is:

$$R_t = \rho(\mathbf{F} \cdot \mathbf{V}^{-1}) = \frac{\alpha}{r_1} + \frac{\beta\epsilon}{r_1 r_2} + \frac{\gamma\zeta}{r_1 r_3} + \frac{\delta\theta\zeta}{r_1 r_3 r_4} + \frac{\delta\epsilon\eta}{r_1 r_2 r_4} \quad (\text{A.15})$$

where $r_1 = \epsilon + \lambda + \zeta$, $r_2 = \eta + \rho$, $r_3 = \kappa + \mu + \theta$ and $r_4 = \nu + \xi$. Note that the expression in Eq. (A.15) derived here in the context of NGM approach is the same with the one in Eq. (18) derived in [25] using a different approach.

Appendix B. The SEIRD and SEInsRD model parameters

The parameter estimation process described in Section 2.2, that was followed to fit the reported data sets of infected, recovered and dead individuals of Italy from February 26 to September 30 in a weekly basis, resulted in the model parameters shown in Fig. B.1. The left panel shows the distribution of the SEIRD model parameters β , σ , γ and μ and the right panel shows the ones of SEInsRD model β_N , β_S , σ , γ , μ_N , μ_S and ss . The values of parameter μ_{TP} of the SEInsRD model are not shown, since they are smaller than 10^{-5} .

Figure B.1 indicates that the parameters expressing the transition from a population group to another attain similar values in both models: transmission rate (β and β_N, β_S), incubation period ($1/\sigma$), recovery rate (γ) and fatality rate (μ and μ_N, μ_S) constants.

As shown in Fig. B.1, the following trends in the parameter values are indicated:

- the transmission rate constant β attains high/low values in the periods where explosive timescale are present/absent. The values of β tend to decrease during the transition from an explosive to a dissipative region and vice-versa.
- the rate constant σ (inverse of incubation period) tend to increases during the explosive regions.

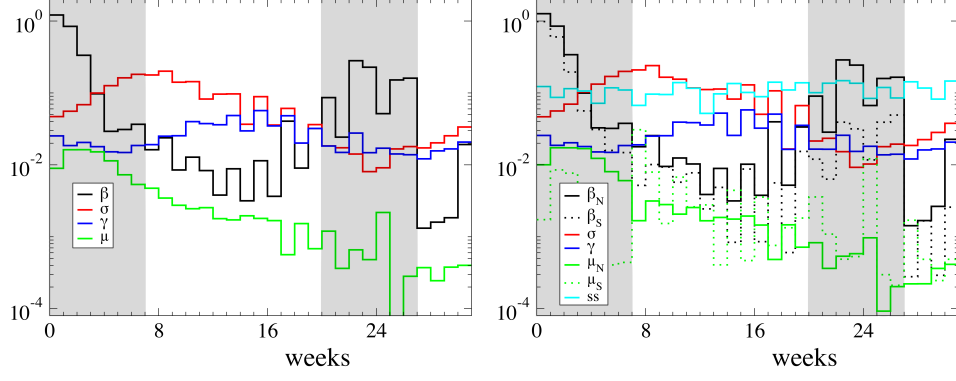


Figure B.1: The parameters estimated for the SEIRD (left) and SEInsRD (right) models. The shaded regions indicate the weeks for which $R_t > 1$ and explosive timescales arise.

- the recovery rates γ are almost constant
- the fatality rates μ tend to decrease, despite the explosive/dissipative region transition. They tend to increase only in the last few weeks.
- the normally to severely infected ratio ss is almost constant.

population group	SEIRD	SEInsRD
infected, I	0.99972	0.99813
recovered, R	0.99993	0.99985
dead, D	0.99998	0.99969

Table B.1: R^2 values of the solution acquired on the basis of the SEIRD and SEInsRD models with the parameter distribution shown in Fig. B.1, with reference to the reported data for infected, recovered and dead individuals in Italy.